Available online at www.sciencedirect.com
ScienceDirect
Journal of Sound and Vibration 325 (2009) 436–450
JOURNAL OF SOUND AND VIBRATION
www.elsevier.com/locate/jsvi

Damped vibration analysis using finite element method with approximated modal damping for automotive double walls with a porous material

T. Yamaguchi[a,*], Y. Kurosawa[b], H. Enomoto[b]

[a]*Department of Mechanical System Engineering, Gunma University, 1-5-1 Tenjin-cho, Kiryu, Gunma 376-8515, Japan*
[b]*Fuji Heavy Industries, Ltd., 1-1 Subarucho, Ota-shi, Gunma 373-8555, Japan*

Received 23 June 2008; received in revised form 9 March 2009; accepted 10 March 2009
Handling Editor: L.G. Tham
Available online 1 May 2009

Abstract

This paper provides a description of damped vibration analysis of automotive double walls with a porous material. The double walls are modeled by using finite element calculations and by considering the damping couplings among various materials. Damped sound fields inside of the porous materials are defined by complex effective density and complex bulk modulus. Particle displacements of the internal air in the porous materials are chosen as unknowns. Displacements in the solid materials for the walls are also formulated using finite elements including complex modulus of elasticity. Thus, displacement vectors are common unknown variables for the coupled equations of motion of the damped structures. By applying asymptotic method to complex eigenvalue problem to obtain modal parameters, expressions of modal loss factor are derived approximately for the three-dimensional structures in coupling between elastic components, viscoelastic components, porous components and environmental gas. This approach helps us to obtain fast computation. The proposed approach and our developed code are verified. Damped vibration of the double walls with a porous layer is computed in consideration of coupling in damping between layers. We discuss modal damping between the layers.

1. Introduction

To reduce interior noise in automobiles, panels in car bodies are treated with vibration damping materials and porous materials. Viscoelastic damping materials are laminated on the body panels to decrease resonant peaks of the panels. Porous materials and interior parts are laminated on the damped body panels to reduce acoustic radiation from the panels. Therefore, the laminated structures correspond to double walls with a porous material.

Recently, finite element models having large degrees of freedom are created for initial digital design of cars before constructing test cars actually. Vibro-acoustic analysis plays one of the important roles of CAE (i.e., computer aided engineering) for cars.

*Corresponding author. Tel.: +81 277 30 1584; fax: +81 277 30 1599.
E-mail address: yamagme4@me.gunma-u.ac.jp (T. Yamaguchi).

0022-460X/$ - see front matter
doi:10.1016/j.jsv.2009.03.018

In high frequency regions of the interior noise, room acoustics [1,2] and SEA (i.e., statistical energy analysis) [3] under diffused sound fields are suitable for the CAE because there are so many resonant peaks in the cabin and the bodies. In the lower frequency regions, FEM (i.e., finite element method) is suitable for the CAE because number of resonant frequencies is small relatively. In the middle frequency regions, much longer computational time requires for FEM because there exists more resonant frequencies than those in the lower frequencies, but there exists not enough number of modes to assume uniform distribution of vibration and sound pressure for SEA etc. Thus, a faster computational method is necessary for the middle frequency regions.

For elastic structures with viscoelastic damping materials, complex modulus of elasticity is generally considered for finite elements analysis of viscoelastic materials. To solve such problems rapidly, the modal strain energy (MSE) method was proposed by Johnson [4,5]. In this method, approximate values of modal loss factors are calculated by means of real eigenvalue analysis using the strain energy of elements and material loss factors of viscoelastic elements. This method can be employed for large-scale finite element models such as automotive bodies [6,7]. We propose an extended version of MSE for obtaining approximated modal loss factors for three-dimensional structures, including porous materials and solid materials. We call this method as modal strain and kinetic energy (MSKE) method. In this method, approximate values of modal loss factors are calculated by means of real eigenvalue analysis using the strain energy and kinetic energy of elements and material loss factors of porous elements. In our previous paper [27], we proposed this method for two-dimensional vibro-acoustic problem. In this report, we extend this method to three-dimensional vibro-acoustic problem. And we apply this method to automotive double walls with a porous material.

2. Numerical methods

We will demonstrate a numerical method for structures, including elastic materials, viscoelastic materials, porous materials, and gas as shown in Fig. 1. In Section 2.1, discretized equations of motion and finite elements for three-dimensional damped internal sound fields in porous materials are provided. In Section 2.2, a finite elements model for the analysis of viscoelastic materials using complex elasticity is provided. Equations expressed in the global coordinate for the coupled structures are explained in Section 2.3. In Section 2.4, the modal strain and kinetic energy method is shown as a fast computation approach to obtain modal loss factors of the coupled damped structures for the three-dimensional damped structures.

2.1. Three-dimensional discrete equations for internal air in porous materials

Discrete equations using finite elements are derived for three-dimensional damped sound field of internal air in porous materials.

Under periodic oscillation and infinitesimal amplitude, the equations of motion of inviscid compressive perfect fluid can be expressed as follows [8–10]:

$$\partial s/\partial x = -\rho\omega^2 u_{fx}, \quad \partial s/\partial y = -\rho\omega^2 u_{fy}, \quad \partial s/\partial z = -\rho\omega^2 u_{fz}. \tag{1}$$

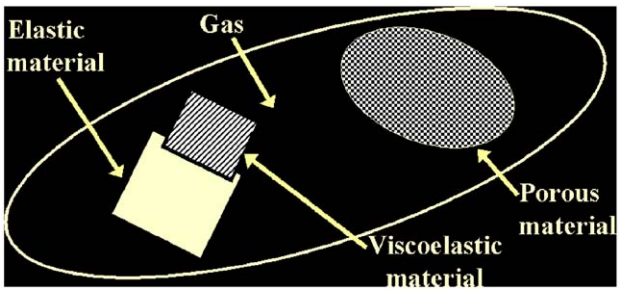

Fig. 1. A damped structure including solid materials, porous materials and gas.

The continuity equation is expressed as follows:

$$s = E(\partial u_{fx}/\partial x + \partial u_{fy}/\partial y + \partial u_{fz}/\partial z). \tag{2}$$

u_{fx}, u_{fy}, and u_{fz} denote the particle displacements along x, y and z directions, respectively. ρ and E denote the effective density and modulus of volume elasticity of the internal air, respectively. ω denotes the angular frequency. In these equations, s denotes the force per unit area. The sign of the force s is positive under expansion. Thus, the relationship between s and pressure p can be expressed as $s = -p$.

Normally, the governing equation for pressure p is utilized by deleting the particle displacements u_{fx}, u_{fy}, and u_{fz} in Eqs. (1) and (2). In this paper, the particle displacements are selected as unknowns [10] by deleting the pressure p in Eqs. (1) and (2). In this formulation, the displacement is selected as the common unknown variable for the structures including elastic/viscoelastic materials, porous materials and gas. This helps us to simplify the superposition of the coupled elements.

The particle displacement vector is set as $\mathbf{u_f} = \{u_{fx}, u_{fy}, u_{fz}\}^{\mathrm{T}}$ in the region of an element. The relationship between $\mathbf{u_f}$ and particle displacement vectors $\mathbf{u_{fe}}$ at nodal points in the element is approximated as

$$\mathbf{u_f} = \mathbf{N_f^T u_{fe}}, \tag{3}$$

where $\mathbf{N_f^T}$ denotes a matrix composed of appropriate shape functions.

The irrotational conditions are as follows:

$$\partial u_{fx}/\partial y - \partial u_{fy}/\partial x = 0, \quad \partial u_{fy}/\partial z - \partial u_{fz}/\partial y = 0, \quad \partial u_{fz}/\partial x - \partial u_{fx}/\partial z = 0. \tag{4}$$

From Eqs. (1)–(4), the kinetic energy $\tilde{T}_f$, strain energy $\tilde{U}_f$, and external work $\tilde{V}_f$ are obtained. By applying the minimum energy principle $\delta(\tilde{U}_f - \tilde{T}_f - \tilde{V}_f) = 0$, the following expressions can be derived:

$$(\mathbf{K_{fe}} - \omega^2 \mathbf{M_{fe}})\mathbf{u_{fe}} = \mathbf{f_{fe}}, \tag{5}$$

$$\mathbf{K_{fe}} = E_e \mathbf{k_{fe}}, \quad \mathbf{M_{fe}} = \rho_e \mathbf{m_{fe}}, \tag{6}$$

where ρ_e and E_e denote the effective density and volume elasticity for media in the region of the elements, respectively. $\mathbf{K_{fe}}$ and $\mathbf{M_{fe}}$ denote the element stiffness matrix and the element mass matrix, respectively. $\mathbf{m_{fe}}$ and $\mathbf{k_{fe}}$ are the matrix consisting of the shape functions and their derivatives. $\mathbf{f_{fe}}$ denotes the nodal force vector. These equations are applicable to gases in acoustical problems without energy dissipation.

Several bulk reacted models have been researched for acoustic fields in porous materials [11–22]. Some models employ the complex effective density ρ_e^* and complex propagation speed c_e^* [14,15]. These parameters for the model can be obtained by using the improved cavity method [13–15] proposed by Utsuno. In this study, we used the following model by using the complex effective density ρ_e^* and complex volume elasticity $E_e^* = \rho_e^*(c_e^*)^2$ for sound fields inside porous materials [16,17]:

$$\rho_e \Rightarrow \rho_e^* = \rho_{e\mathrm{R}} + \mathrm{j}\rho_{e\mathrm{I}}, \tag{7}$$

$$E_e \Rightarrow E_e^* = E_{e\mathrm{R}} + \mathrm{j}E_{e\mathrm{I}}, \tag{8}$$

where j denotes the imaginary unit; $\rho_{e\mathrm{R}}$ and $\rho_{e\mathrm{I}}$ denote the real and imaginary parts of ρ_e^*, respectively. The imaginary part $\rho_{e\mathrm{I}} = -R/\omega$ is related with the flow resistance R [27]. $E_{e\mathrm{R}}$ and $E_{e\mathrm{I}}$ represent the real and imaginary parts of E_e^*, respectively. The authors verified that this model is effective for automotive fibrous materials [16,17]. Kiyota [23] reported that the behaviors of internal air in porous materials can be assumed to be the factors that govern for such automotive fibrous materials. Therefore, the elastic waves [12,18–20] through the resin fiber of the porous materials are neglected in this report.

Element mass matrix $\mathbf{M_{fe}}$ can be obtained by substituting Eq. (7) into Eq. (6).

$$\mathbf{M_{fe}} = \mathbf{M_{Rfe}}(1 + \mathrm{j}\chi_e), \tag{9}$$

$$\chi_e = \rho_{e\mathrm{I}}/\rho_{e\mathrm{R}}. \tag{10}$$

In these equations, $\mathbf{M_{Rfe}}$ denotes the real part of the element mass matrix $\mathbf{M_{fe}}$. $\rho_{e\mathrm{I}}$ denotes the imaginary part of the effective density, and $\chi_e = \rho_{e\mathrm{I}}/\rho_{e\mathrm{R}}$ is associated with the damping effect due to flow resistance.

By substitution Eq. (8) into Eq. (6), the following element stiffness matrix $[K]_{fe}$ is obtained:

$$\mathbf{K_{fe}} = \mathbf{K_{Rfe}}(1 + \mathrm{j}\eta_e), \tag{11}$$

$$\eta_e = E_{e\mathrm{I}}/E_{e\mathrm{R}}. \tag{12}$$

In Eq. (11), $\mathbf{K_{Rfe}}$ represents the real part of the element stiffness matrix $\mathbf{K_{fe}}$. In Eq. (12), η_e represents the damping effect due to hysteresis between volume strain and pressure in the porous materials.

It must be noted that both the element stiffness matrix $\mathbf{K_{fe}}$ and the element mass matrix $\mathbf{M_{fe}}$ for internal gas in the porous materials have complex quantities.

We can use this model for space filled with air if small values for damping parameters χ_e and η_e are provided.

2.2. Discretized equation for vibration in solid materials with damping

For analyzing vibrations in solid materials such as elastic materials and viscoelastic materials, we used the following discretized equations from (13) to (19). The equations correspond to the conventional linear finite element model with regard to hysteresis damping [24].

The stress–strain relationship for solid materials can be expressed as follows:

$$\boldsymbol{\sigma} = \mathbf{D}\boldsymbol{\varepsilon}. \tag{13}$$

The strain–displacement relationship for solid materials is expressed as follows:

$$\boldsymbol{\varepsilon} = \mathbf{A}\mathbf{u_s}, \tag{14}$$

where $\boldsymbol{\sigma}$ denotes the stress vector; $\boldsymbol{\varepsilon}$ the strain vector; and $\mathbf{u_s}$ the displacement vector. $\mathbf{A}$ represents the matrix consisting of differential operators. $\mathbf{D}$ represents the matrix involving the modulus of elasticity and Poisson's ratio.

By using the following matrix $\mathbf{N_s^T}$ including shape functions, the relationship between displacement $\mathbf{u_s}$ in an element and nodal displacements $\mathbf{u_{se}}$ can be approximated as follows:

$$\mathbf{u_s} = \mathbf{N_s^T}\mathbf{u_{se}}. \tag{15}$$

By using equations from (13) to (15), the kinetic energy $\tilde{T}_s$, strain energy $\tilde{U}_s$ and external work $\tilde{V}_s$ are evaluated. By applying the minimum energy principle $\delta(\tilde{U}_s - \tilde{T}_s - \tilde{V}_s) = 0$, the following equation can be obtained:

$$(\mathbf{K_{se}} - \omega^2\mathbf{M_{se}})\mathbf{u_{se}} = \mathbf{f_{se}}, \tag{16}$$

where $\mathbf{K_{se}}$ and $\mathbf{M_{se}}$ denote the element stiffness matrix and the element mass matrix for solid materials, respectively, and $\mathbf{f_{se}}$ represents the nodal force vector in an element e for solid materials.

Solid materials with damping (i.e., viscoelastic materials) can be modeled by using finite elements [4,5,25] and by replacing the complex modulus of elasticity with Young's modulus in the matrix $\mathbf{D}$ in Eq. (13). As a result, the element stiffness matrix $\mathbf{K_{se}}$ in Eq. (16) is complex as follows:

$$\mathbf{K_{se}} = \mathbf{K_{Rse}}(1 + \mathrm{j}\eta_e). \tag{17}$$

In this equation, η_e denotes the material loss factor corresponding to each element e, and $\mathbf{K_{Rse}}$ denotes the real part of the element stiffness matrix for the solid materials.

2.3. Discretized equation in the global system

We superpose all elements of the entire structure containing air, porous materials, and solid materials by using Eqs. (5)–(17). Then, the following discretized equations in the global system can be obtained:

$$\sum_{e=1}^{e\,\max} (\mathbf{K_{Re}}(1 + \mathrm{j}\eta_e) - \omega^2\mathbf{M_{Re}}(1 + \mathrm{j}\chi_e))\mathbf{u_e} = \mathbf{f}, \tag{18}$$

where $\mathbf{f}$ denotes the nodal force vector, and $\mathbf{u_e}$ denotes the nodal displacement vector in the global system. $\mathbf{u_e}$ includes $\mathbf{u_{se}}$ and $\mathbf{u_{fe}}$. $\mathbf{K_{Re}}$ contains $\mathbf{K_{Rfe}}$ and $\mathbf{K_{Rse}}$, and $\mathbf{M_{Re}}$ contains $\mathbf{M_{Rfe}}$ and $\mathbf{M_{Rse}}$. $e_{\max}$ represents the total number of elements. The size of these matrix and vectors in Eq. (18) is corresponds to the number of the degrees of freedoms for the global structures. At interfaces between solid materials and air, and at interfaces between solid materials and porous materials, the normal components of velocity to the interfaces are continuous when the Eq. (18) is superposed. On the contrary, the tangential components of velocity along the interfaces are independent.

In Eq. (18), both the stiffness matrix and mass have complex quantities.

2.4. Fast algorithm to obtain modal damping

Considering resonant conditions, homogeneous equations of Eq. (18) are expressed as follows:

$$\sum_{e=1}^{e\max}(\mathbf{K_{Re}}(1+\mathrm{j}\eta_e)-(\omega^{(n)})^2(1+\mathrm{j}\eta_{\mathrm{tot}}^{(n)})\mathbf{M_{Re}}(1+\mathrm{j}\chi_e))\boldsymbol{\phi}^{(\mathbf{n})*}=\mathbf{0}. \tag{19}$$

This corresponds to a complex eigenvalue problem. In this equation, superscript (n) denotes the nth eigenmode, $\boldsymbol{\phi}^{(\mathbf{n})^*}$ represents the complex eigenvector, $\eta_{\mathrm{tot}}^{(n)}$ represents the modal loss factor, and $(\omega^{(n)})^2$ denotes the real part of the complex eigenvalue.

The following parameters β_{ke} and β_{se} are introduced:

$$\beta_{se}=\eta_e/\eta_{\max},\quad \beta_{se}\leqslant 1,\quad \beta_{ke}=\chi_e/\eta_{\max},\quad \beta_{ke}\leqslant 1, \tag{20}$$

where $\eta_{\max}$ represents the maximum value among the elements' material loss factors η_e and χ_e, $(e=1,2,3,\ldots,e_{\max})$. Under the assumption that $\eta_{\max}\ll 1$, solutions of complex eigenvalue Eq. (19) are expanded by using a small parameter $\mu=\mathrm{j}\eta_{\max}$ [5]:

$$\boldsymbol{\phi}^{(\mathbf{n})^*}=\boldsymbol{\phi}_0^{(\mathbf{n})}+\mu\boldsymbol{\phi}_1^{(\mathbf{n})}+\mu^2\boldsymbol{\phi}_2^{(\mathbf{n})}+\cdots, \tag{21}$$

$$(\omega^{(n)})^2=(\omega_0^{(n)})^2+\mu^2(\omega_2^{(n)})^2+\mu^4(\omega_4^{(n)})^2+\cdots, \tag{22}$$

$$\eta_{\mathrm{tot}}^{(n)}=\mu\eta_1^{(n)}+\mu^3\eta_3^{(n)}+\mu^5\eta_5^{(n)}+\cdots. \tag{23}$$

From Eqs. (21)–(23), by considering $\beta_{ke}\leqslant 1$, $\beta_{se}\leqslant 1$ and $\eta_{\max}\ll 1$ into consideration, $\eta_{\max}\beta_{ke}\ll 1$ and $\eta_{\max}\beta_{se}\ll 1$ are obtained. Therefore, we can regard both $\mu\beta_{se}$ and $\mu\beta_{ke}$ as small parameters. In the abovementioned equations, $\boldsymbol{\phi}_0^{(\mathbf{n})}+\boldsymbol{\phi}_1^{(\mathbf{n})}+\boldsymbol{\phi}_2^{(\mathbf{n})},\ldots$ and $(\omega_0^{(n)})^2,(\omega_2^{(n)})^2,(\omega_4^{(n)})^2,\ldots$, and $\eta_1^{(n)},\eta_3^{(n)},\eta_5^{(n)},\ldots$ are real.

We substitute equations from Eqs. (21)–(23) into Eq. (19) , and we can obtain the successive equations that the asymptotic solutions must satisfy:

μ^0 order:

$$\sum_{e=1}^{e\max}(\mathbf{K_{Re}}-(\omega_0^{(n)})^2\mathbf{M_{Re}})\boldsymbol{\phi}_{\mathbf{0}}^{(\mathbf{n})}=\mathbf{0}. \tag{24}$$

μ^1 order:

$$\sum_{e=1}^{e\max}(\mu\beta_{se}(\mathbf{K_{Re}}-\mu\eta_1^{(n)}(\omega_0^{(n)})^2\mathbf{M_{Re}}-\mu\beta_{ke}(\omega_0^{(n)})^2\mathbf{M_{Re}})\boldsymbol{\phi}_{\mathbf{0}}^{(\mathbf{n})}+\sum_{e=1}^{e\max}(\mu\mathbf{K_{Re}}-\mu(\omega_0^{(n)})^2\mathbf{M_{Re}})\boldsymbol{\phi}_{\mathbf{0}}^{(\mathbf{n})}=\mathbf{0}. \tag{25}$$

By arranging Eqs. (24)–(25), the following equation can be derived:

$$\eta_{\mathrm{tot}}^{(n)}=\sum_{e=1}^{e\max}(\eta_e S_{se}^{(n)})-\sum_{e=1}^{e\max}(\chi_e S_{ke}^{(n)}),$$

$$S_{se}^{(n)}=\boldsymbol{\phi}_{\mathbf{0}}^{(\mathbf{n})\mathrm{T}}\mathbf{K_{Re}}\boldsymbol{\phi}_{\mathbf{0}}^{(\mathbf{n})}\Big/\sum_{e=1}^{e\max}\boldsymbol{\phi}_{\mathbf{0}}^{(\mathbf{n})\mathrm{T}}\mathbf{K_{Re}}\boldsymbol{\phi}_{\mathbf{0}}^{(\mathbf{n})},$$

$$S_{ke}^{(n)} = \boldsymbol{\phi}_{\mathbf{0}}^{(\mathbf{n})\mathrm{T}} \mathbf{M}_{\mathbf{Re}} \boldsymbol{\phi}_{\mathbf{0}}^{(\mathbf{n})} \Big/ \sum_{e=1}^{e\max} \boldsymbol{\phi}_{\mathbf{0}}^{(\mathbf{n})\mathrm{T}} \mathbf{M}_{\mathbf{Re}} \boldsymbol{\phi}_{\mathbf{0}}^{(\mathbf{n})}. \tag{26}$$

Eigenmodes $\boldsymbol{\phi}_{\mathbf{0}}^{(\mathbf{n})}$ in Eq. (26) are real. The eigenmodes $\boldsymbol{\phi}_{\mathbf{0}}^{(\mathbf{n})}$ are obtained by solving the real eigenvalue equation (24). According to Eq. (26), the modal loss factor $\eta_{\mathrm{tot}}^{(n)}$ can be computed from η_e, χ_e, $S_{se}^{(n)}$, and $S_{ke}^{(n)}$. η_e denotes the damping parameter for each element e concerning elasticity E_e^*, χ_e denotes the damping parameter for each element e concerning effective density ρ_e^*, $S_{se}^{(n)}$ represents a share of strain energy of each element to the total strain energy, and $S_{ke}^{(n)}$ represents a share of the kinetic energy of each element to the total kinetic energy.

By using this algorithm, we can decrease the computational time required for calculating the modal damping and responses for finite element models of the damped structures with large degrees of freedom.

Corresponding to the proposed method described in Sections 2.1–2.4, program codes are developed. In the latter chapter, we will describe the verification of the proposed method, and then, we will investigate the damping couplings between solid materials and porous materials.

3. Verification of the proposed numerical method for three-dimensional structures

We developed program codes for three-dimensional structures by following the proposed fast algorithm described in Sections 2.1–2.4. Hereafter, we will verify the proposed methods and the codes.

3.1. Numerical conditions

We used isoparametric hexagonal elements [24] for porous materials and air. These elements have eight nodes. The shape function $\mathbf{N}_{\mathbf{f}}^{\mathrm{T}}$ in Eq. (3) includes $N_1, N_2, \ldots, N_8$ in

$$N_1 = (1-\xi)(1-\eta)(1-\zeta)/8, \quad N_2 = (1+\xi)(1-\eta)(1-\zeta)/8, \quad N_3 = (1+\xi)(1+\eta)(1-\zeta)/8,$$

$$N_4 = (1-\xi)(1+\eta)(1-\zeta)/8, \quad N_5 = (1-\xi)(1-\eta)(1+\zeta)/8, \quad N_6 = (1+\xi)(1-\eta)(1+\zeta)/8,$$

$$N_7 = (1+\xi)(1+\eta)(1+\zeta)/8, \quad N_8 = (1-\xi)(1+\eta)(1+\zeta)/8, \tag{27}$$

where $N_1, N_2, \ldots, N_8$ have the same form with basis functions that represent the mapping between an element coordinate $x_e y_e z_e$ of metric space and a coordinate of parametric space $\xi\eta\zeta$.

We used isoparametric hexagonal elements [24,26] with non-conforming modes for solid materials with damping. These elements have also eight nodes. The shape function $\mathbf{N}_{\mathbf{s}}^{\mathrm{T}}$ in Eq. (3) includes $N_1, N_2, \ldots, N_8$ in Eq. (27). The following $N_9, N_{10}, \ldots, N_{12}$ are added as non-conforming modes [26]:

$$N_9 = (1-\xi^2), \quad N_{10} = (1-\eta^2), \quad N_{11} = (1-\zeta^2), \quad N_{12} = (1-\xi^2)(1-\eta^2)(1-\zeta^2). \tag{28}$$

We used $\rho_R = 1.4\,\mathrm{kg\,m^{-3}}$, $\chi_e = -0.5$ for the complex effective density for the porous material. The complex volume elasticity was set as $E_R = 1.19 \times 10^5\,\mathrm{N\,m^{-2}}$, $\eta_e = 0.1$. We used $\rho_R = 1.2\,\mathrm{kg\,m^{-3}}$, $\chi_e = -0.001$, $E_R = 1.4 \times 10^5\,\mathrm{N\,m^{-2}}$, and $\eta_e = 0.001$ for space filled with air.

3.2. Computational accuracy of the proposed FEM

3.2.1. Verification using an acoustic tube filled with a porous material

We insert a porous material into an acoustic tube model as shown in Fig. 2. Both the ends of the tube are closed. Backing air is allowed between the porous material and one end of the tube. The thickness of the porous material is 20 mm, and the thickness of the backing air is 35 mm. We set the sidewalls of the tube to be rigid. Thus, normal components of the particle velocities to the walls are set as zero. On the other hand, the tangential components of the particle velocities along the walls are free. A sound source and observation points 1 and 2 are shown in the figure. By using the proposed algorithm and the developed codes, we compute the particle velocity v_1 at observation point 1 and the particle velocity v_2 at observation point 2. Eq. (18) is solved by using skyline method to obtain the particle velocities in the tube. Moreover, a transfer function $H_v = v_1/v_2$ is calculated from v_1 and v_2. Further, the normal incidence sound absorption coefficient using H_v

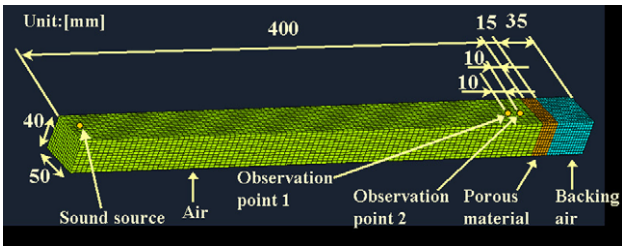

Fig. 2. Three-dimensional finite element model for a closed pipe filled with a porous material.

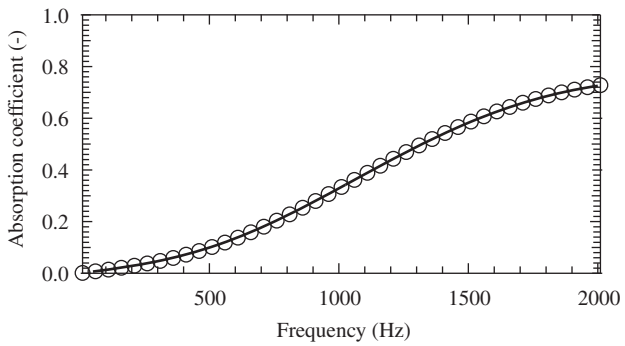

Fig. 3. Sound absorption coefficient for a closed pipe filled with a porous material: theoretical results, — and numerical results using the proposed finite element method, ○.

by using the two microphones method [13]. The results obtained from the calculations are compared with the theoretical results obtained by using the transfer matrix method [13]. Both the results are shown in Fig. 3. From Fig. 3, the theoretical results and numerical results obtained by using the proposed FEM are consistent. This confirms the validity of the finite elements for the porous media described in Section 2.1.

In the original two microphones method [13] proposed by Utsuno et al., the transfer function $H_p = p_1/p_2$ between sound pressure p_1 at the point 1 and sound pressure p_2 at the point 2 was used. In our previous paper [27], we extended this method by using $H_v = v_1/v_2$ and used in this report.

3.2.2. *Accuracy for structures containing a viscoelastic material*

A viscoelastic material (thickness of 2 mm) is laminated on a steel flat plate (thickness of 0.7 mm). All the edges of the laminated plate are clamped. The length of the long edges is 126 mm, and the length of the short edges is 112 mm. Modal loss factors of the plate are calculated by using Eq. (26). For the viscoelastic layer, material loss factor η_e is 0.333, storage modulus of elasticity is $1.00 \times 10^9\,\mathrm{N\,m^{-2}}$, and the mass density is $1.45 \times 10^3\,\mathrm{kg\,m^{-3}}$. The modal loss factors for the plate are depicted in Fig. 4. The modal loss factors $\eta_{\mathrm{tot}}^{(n)}$ obtained by using the finite element method agree well with theoretical results obtained by using the Oberst equation [25]. This confirms the validity of the finite element model for solid materials with damping described in Section 2.2.

3.2.3. *Accuracy for the damped structures (gas+porous material+solid materials)*

As shown in Fig. 5, porous materials, a steel strip, and a viscoelastic strip are inserted in the closed pipe. The thickness of the steel strip is 1 mm and the thickness of the viscoelastic strip is 1 mm. The normal velocity to the boundaries between the strips and the sidewalls of the pipe is set as zero. Both the steel strip and the viscoelastic strip can move without gap and friction along the sidewalls of the pipe. The cross-section of the pipe is rectangular. The size of the cross-section of the pipe is so small that the strips behave like mass without elastic deformation within a low frequency range. By using the proposed FEM, sound absorption coefficients under normal incidence are computed. Fig. 6 represents the calculated results. In the figure, theoretical values

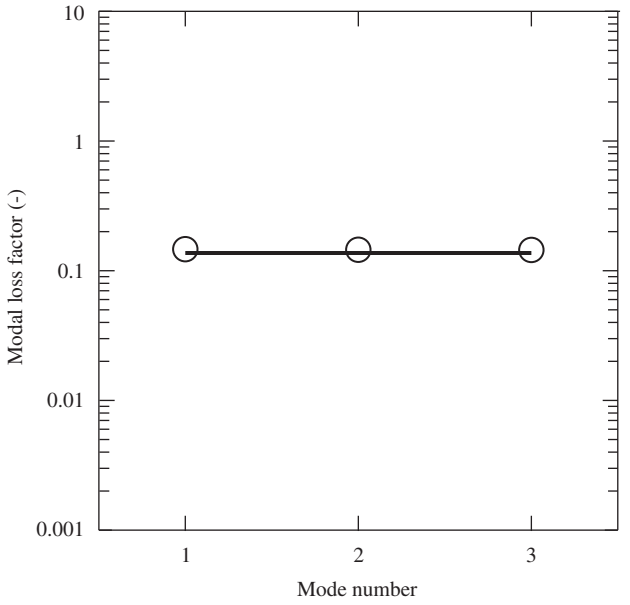

Fig. 4. Modal loss factors of a steel flat plate laminated with a viscoelastic material: theoretical results (by Oberst equation), — and numerical results using the proposed finite element method, ○.

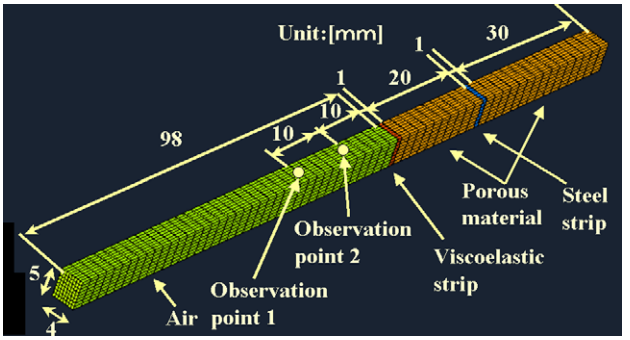

Fig. 5. Three-dimensional finite element model for a closed pipe filled with porous materials and solid strips.

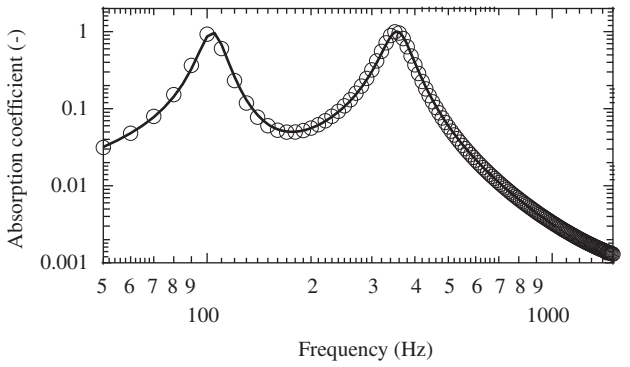

Fig. 6. Sound absorption coefficient for a closed pipe filled with porous materials and solid strips: theoretical results, — and numerical results using the proposed finite element method, ○.

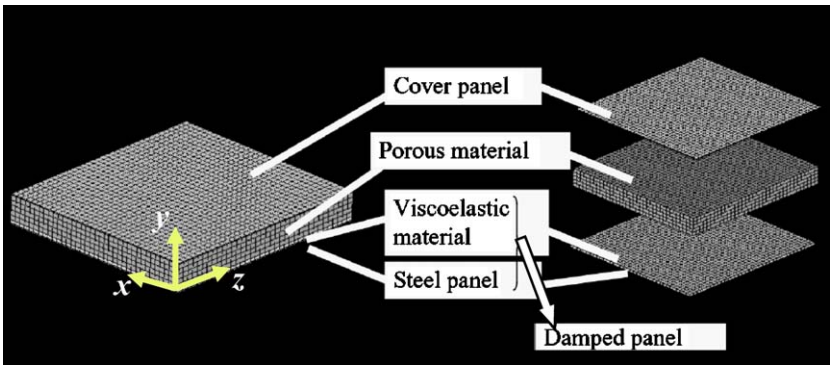

Fig. 7. Three-dimensional finite element model for double walls with a porous material.

of absorption coefficient are calculated by using the transfer matrix method [13]. For the transfer matrix method, the strips are modeled according their mass due to their mechanical impedances. In this figure, theoretical results and the results obtained from the proposed finite element method coincide well. This confirms the validity of Eq. (18) for the damped structures with porous materials described in Section 2.3.

3.3. Damped responses and modal loss factors for automotive double walls with a porous material

We investigate modal couplings in damping and rigidity between solid layers (elastic layers and a viscoelastic layer) and a porous layer by using FEM models of double walls with a porous material. Fig. 7 shows a numerical model used for the investigation. A viscoelastic damping material is laminated on a steel rectangular flat plate (126 mm × 112 mm). The thickness of the damping material is 2 mm, and the thickness of the steel plate is 0.7 mm. Hereafter, we call this laminated panel a damped plate. This damped plate has the same shape and same clamped edges as described in Section 3.2.2. Furthermore, a porous material and another steel sheet are laminated on the damped panel. We call the added steel sheet a cover plate. The thickness of the porous material is 15 mm, and the thickness of the cover plate is 0.6 mm. The porous layer is sandwiched between the damped panel and the cover plate. This corresponds to double walls with sound absorbing materials. The boundary conditions of the damped panel and the cover plate are set according to the automotive use. All edges of the steel layer are clamped. On the other hand, all edges of the cover plate are set as free boundaries. The sidewalls of the porous layer are regarded as rigid walls. At the rigid walls, normal components of the particle velocities in the porous layer to the walls are set as zero. The tangential components of the velocities are free at the rigid walls. At the interface between the damped plate and the porous layer, normal components of the particle velocities in the porous layer to the interface are continuous up to the normal components of the velocity of the damped plate. Similarly, the normal components of the particle velocity are continuous up to the normal components of the velocity of the cover plate. At these interfaces, the tangential components of the velocities to the interfaces exist independently, both in the porous layer, damped panel, and cover plate.

The storage modulus of elasticity, material loss factor, and mass density of the viscoelastic layer are $1.00\times10^{9}\,\mathrm{N\,m^{-2}}$, 0.333, and $1.45\times10^{3}\,\mathrm{kg\,m^{-3}}$, respectively. For the porous layer, we used $\rho_{e\mathrm{R}}=1.4\,\mathrm{kg\,m^{-3}}$, $\chi_e=\rho_{e\mathrm{I}}/\rho_{e\mathrm{R}}=-0.5$ as the complex effective density and used $E_{e\mathrm{R}}=1.19\times10^{5}\,\mathrm{N\,m^{-2}}$, $\eta_e=E_{e\mathrm{I}}/E_{e\mathrm{R}}=0.1$ as the complex bulk modulus. The material loss factor of the steel layer is set as 0.001.

The steel plain plate is excited at the point as shown in Fig. 7. The coordinate of the excitation point is $(x, y, z)=(21.8, 0, 21.0)$. The waveform corresponding to the excitation is that of white noise. We evaluated the averaged acceleration α_{av} over the entire surface of the cover plate to determine the vibration isolation performance.

The averaged acceleration level (case 1) for the double walls with the sound absorbing material is shown in Fig. 8. In this figure, the averaged acceleration level (case 2) is shown. The cover plate for case 2 has a higher material damping $\eta_e=0.1$ than material damping $\eta_e=0.001$ for case 1. Further, there exists the averaged

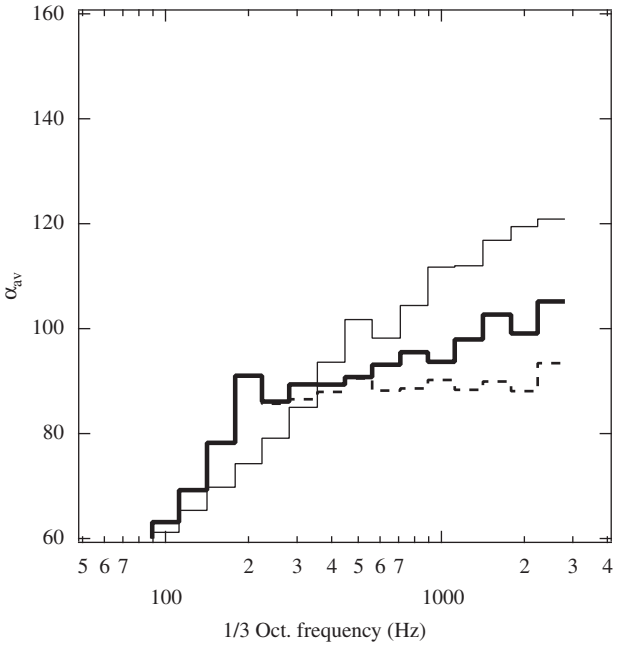

Fig. 8. Averaged acceleration level of the double walls with the porous material: case 1 (steel 0.7 mm + viscoelastic material 2 mm + porous material 15 mm + cover 0.6 mm, damping of the cover = 0.001), ——; case 2 (steel 0.7 mm + viscoelastic material 2 mm + porous material 15 mm + cover 0.6 mm, damping of the cover = 0.1), - - -; and case 3 (steel 0.7 mm + viscoelastic material 2 mm), —.

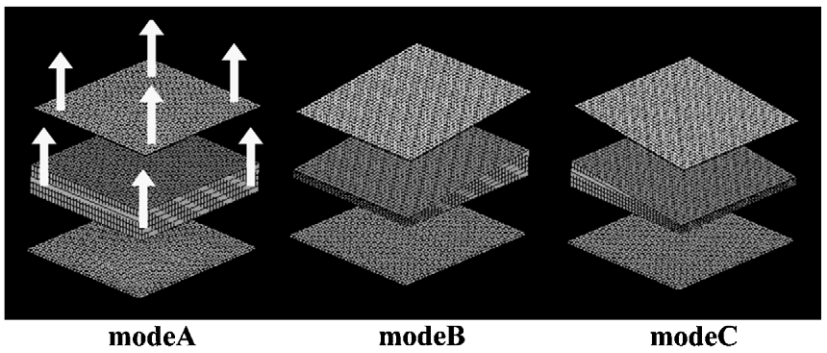

Fig. 9. Eigenmodes of the double walls with the porous material.

acceleration level (case 3) over the surface of the damped panel without the porous layer and the cover plate. By comparing case 3 with case 1 in Fig. 8, the averaged vibration level for case 1 is larger than that for case 3 in the 200-Hz frequency band. In this frequency region, the vibration level increases due to the lamination of the porous layer and cover plate. This frequency corresponds to the resonance at the low frequency resonance for double walls. On the contrary, in the higher frequency region, the vibration level for case 3 is smaller than that for case 1 due to vibration isolation. If the material loss factor of the cover plate increases from $\eta_e = 0.001$ (case 1) to $\eta_e = 0.1$ (case 2), the vibration isolation effect increases. However, small effects occur in the 200-Hz band. We will investigate this phenomenon in detail. Fig. 9 shows the eigenvectors of the double walls with the porous layer for case 1. There exist three modes (mode A, mode B, mode C) in the vicinity of the resonance in the 200-Hz band. For the mode A including translation toward the y-direction, the resonance frequency is 202 Hz and the modal loss factor $\eta_{\mathrm{tot}}^{(n)}$ is 0.10. For the mode B including rotation about the x-axis, the resonant frequency is 212 Hz and the modal loss factor $\eta_{\mathrm{tot}}^{(n)}$ is 0.10. The resonant frequency is 213 Hz and the modal loss factor $\eta_{\mathrm{tot}}^{(n)}$ is 0.10 for the mode C including rotation about the z-axis. In these three modes, the motions of the

cover plate can be regarded to be rigid because no elastic deformations occur in the eigenmodes. Elastic deformations for these modes mainly appear in the porous layer. On the other hand, there exist slight elastic deformations in the damped panel. From these results, the cover plate corresponds to the mass, and the porous layer corresponds to the spring in these modes. As described before, the modal loss factors $\eta_{\mathrm{tot}}^{(n)}$ for all three modes is 0.1. This value corresponds to the material loss factor $\eta_e = 0.10$ of the porous layer due to hysteresis between the pressure and the volume strain. Therefore, we can state that the damping effects due to complex bulk modulus appear because of the complex spring for the porous layer. Modes A, B, and C become rigid modes if the cover plate does not have the porous layer and the damped panel under such conditions. The corresponding resonant frequencies and modal loss factors become zero. Thus, the resonant frequencies increase and vibration damping increases when the cover plate floats on the porous layer. This is due to the coupling effects in rigidity and damping between the layers.

Modes D, E, and F in Fig. 10 are the typical examples of eigenmodes including large elastic deformations of the cover plate. In mode D, the resonant frequency is 260 Hz, and the modal loss factor $\eta_{\mathrm{tot}}^{(n)}$ is 0.071. In mode E, the resonant frequency is 1120 Hz, and the modal loss factor $\eta_{\mathrm{tot}}^{(n)}$ is 0.071. In mode F, the resonant frequency is 2030 Hz, and the modal loss factor $\eta_{\mathrm{tot}}^{(n)}$ is 0.0037. The modal loss factors $\eta_{\mathrm{tot}}^{(n)}$ of modes D, E, and F have values lying between the material loss factor $\eta_e = 0.001$ of the cover plate and the material loss factor $\eta_e = 0.1$ of the porous layer due to the complex bulk modulus. By considering eigenmodes (mode D′, mode E′, and mode F′ in Fig. 11 for the cover plates corresponding to eigenmodes (modes D, E, and F) in Fig. 10 under free edges without the porous layer and without the damped panel, the related resonant frequencies (143 Hz for mode D′, 1090 Hz for mode E′, 2010 Hz for mode F′, respectively) become lower, and the related modal loss factors $\eta_{\mathrm{tot}}^{(n)}$ (0.001 for mode D′, 0.001 for mode E′, 0.001 for mode F′, respectively) become smaller than those of eigenmodes (modes D, E and F) for the double walls with the porous layer.

Modes G, H, and I as shown in Fig. 12 are the typical examples of eigenmodes having large elastic deformations in the damped panel. In mode G, the resonant frequency is 519 Hz, and the modal loss factor $\eta_{\mathrm{tot}}^{(n)}$ is 0.14. In mode H, the resonant frequency is 1074 Hz, and the modal loss factor $\eta_{\mathrm{tot}}^{(n)}$ is 0.14. In mode I, the resonant frequency is 1950 Hz, and the modal loss factor $\eta_{\mathrm{tot}}^{(n)}$ is 0.14. These modal loss factors $\eta_{\mathrm{tot}}^{(n)}$ have the same values as the theoretical value 0.14 obtained by using the Oberst's equation [25]. For the damped panel without the porous layer and without the cover plate, the resonant frequencies corresponding to mode G″, mode H″, and mode I″ (as shown in Fig. 13), are 488 Hz (modal loss factor $\eta_{\mathrm{tot}}^{(n)} = 0.14$), 1060 Hz (modal loss

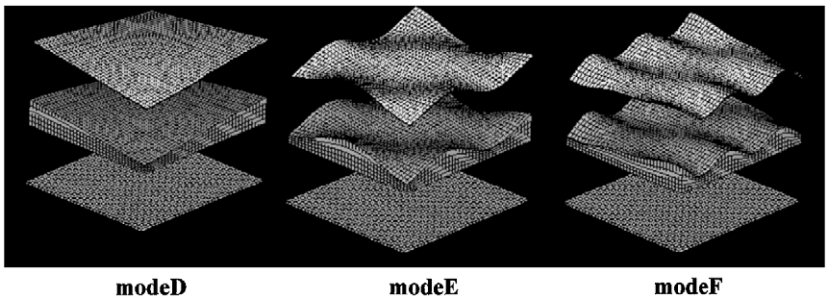

Fig. 10. Eigenmodes of the double walls with the porous material.

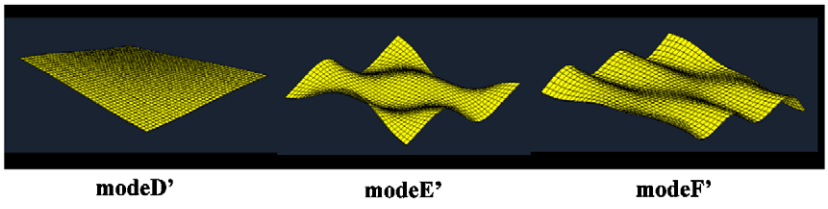

Fig. 11. Eigenmodes of the cover plate without the porous material and without the damped panel.

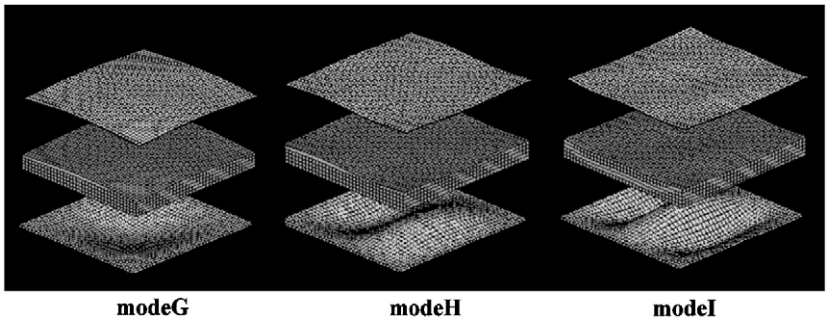

Fig. 12. Eigenmodes of the double walls with the porous material.

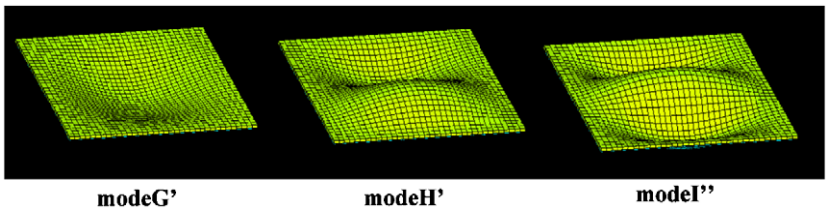

Fig. 13. Eigenmodes of the damped panel without the porous material and without the cover plate.

factor $\eta_{\mathrm{tot}}^{(n)} = 0.14$) and 1940 Hz (modal loss factor $\eta_{\mathrm{tot}}^{(n)} = 0.14$), respectively. Modes G″, H″, and I″ contain similar deformations in the damped panel to the deformations in modes G, H, and I as shown in Fig. 12. In these cases, there exist slight variations between modes G and G″, between modes H and H″, and between I and I″ on the resonant frequencies and the modal loss factors $\eta_{\mathrm{tot}}^{(n)}$ due to the lamination of the porous layer and the cover plate. Therefore, the influence of the porous layer on the modes including large deformations in the cover plate is significantly as compared to that on modes including large deformations in the damped panel. These phenomena are caused by the difference in rigidity due to boundary conditions. The cover plate with free edges has low rigidity that the rigidity and damping of the porous layer are affected easily. On the other hand, the damped panel with the fixed edges has high rigidity that the rigidity and damping of the porous layer cannot be affected easily.

For modes G, H, and I as illustrated in Fig. 12, there is small transmission of elastic deformations from the damped panel to the cover plate. The cover plate moves different motions from the motions of the damped plate for these modes. From the response in Fig. 8, the response of case 3 (i.e., the case of the damped panel alone) shows large amplitudes near the resonant frequencies corresponding to modes G, H, and I, whereas the response of case 1 (i.e., the case of the double walls with the porous layer) decreases near these resonances due to the isolation effect of the porous material.

Mode J in Fig. 14 is the first spatial mode along the z-direction in air inside the porous layer. This mode in Fig. 14 corresponds to distribution of the particle displacements of internal air in the porous layer. In this figure, the white regions represent large particle displacement, and the dark regions represent small particle displacement. Nodes of the mode appear at both edges along the z-direction, and an anti-node appears at the midpoint along the z-direction. The resonant frequency of mode J is identical to the resonant frequency 1300 Hz of the porous layer without the damped layer and without the cover plate under a closed space. Moreover, the modal loss factor $\eta_{\mathrm{tot}}^{(n)}$ for this mode is 0.6. This value is identical to the sum of the material loss factor $\eta_e = 0.1$ due to the complex bulk modulus and the material loss factor χ_e due to the complex effective density for the porous layer. These phenomena reveal that y-components v_{fy} of the particle velocity in the porous layer in this mode are so small that v_{fy} does not have a coupling effect with y-components of vibration velocity of the damped panel and the cover plate. Therefore, this mode cannot affect the vibration isolation. Similarly, mode K in Fig. 14 is the first spatial mode along the x-direction in air inside the porous layer. This mode does not influence the vibration isolation, too.

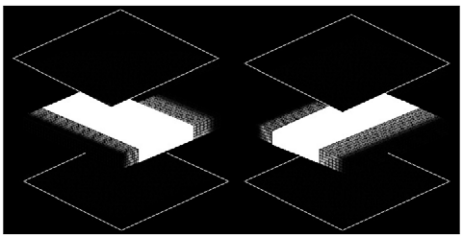

Fig. 14. Eigenmodes of the double walls with the porous material.

By increasing the material loss factor of the cover plate to $\eta_e = 0.1$ for case 2 from $\eta_e = 0.001$ for case 1, the modal loss factors $\eta_{\mathrm{tot}}^{(n)}$ increase for the modes (D, E, and F), including large deformations of the cover plate. For mode D, the modal loss factor $\eta_{\mathrm{tot}}^{(n)}$ increases from 0.071 for case 1 to 0.10 for case 2. For mode E, the modal loss factor $\eta_{\mathrm{tot}}^{(n)}$ increases from 0.0071 for case 1 to 0.10 for case 2. For mode F, the modal loss factor $\eta_{\mathrm{tot}}^{(n)}$ increases from 0.0037 for case 1 to 0.10 for case 2.

For the modes A, B, and C, including rigid motions of the cover plate in the 200 Hz band, the related modal loss factors $\eta_{\mathrm{tot}}^{(n)}$ cannot increase significantly due to the increment in the material loss factor of the cover plate from $\eta_e = 0.001$ to 0.1 because there are no elastic deformations of the cover plate in modes A, B, and C. These phenomena indicate that there exists no difference between the peaks of the response in the 200 Hz band in Fig. 8 between for cases 1 and 2 with larger material damping of the cover plate. In the same manner, by increasing the material loss factor in the cover plate from $\eta_e = 0.001$ to 0.1, modal loss factors $\eta_{\mathrm{tot}}^{(n)}$ cannot increase for modes G, H, and I with large deformations in the damped panel and for the spatial mode J in the porous layer.

3.4. Investigating the validity of the modal parameters by using the proposed method (MSKE method: modal strain and kinetic energy method)

We investigate the validity of the proposed method by using the MSKE method (i.e., modal strain and kinetic energy method). Fig. 15 represents the transfer functions (i.e., |acceleration/force| = $|A/F|$) of the damped structure as we have stated in Section 3.3. The shape, boundary conditions, and materials for the damped structure are identical with the model, as shown in Fig. 7, except for the damping parameters (η_e,χ_e) of the porous material. For the porous material, the damping parameter χ_e related to acoustic resistance is varied under a constant value $\eta_e = 0.1$ in the graphs on the left side of Fig. 15. On the contrary, the damping parameter η_e related to volume elasticity is varied under constant $-\chi_e = 0.1$ in the graphs on the right side of Fig. 15. The observation point on the cover plate is $(x, y, z) = (21.8, 18.3, 21.0)$. The excitation point is at the same place as that shown in Fig. 7. In the figure, the solid lines represent the frequency responses using the modal parameters from the proposed method (i.e., MSKE method) explained in Section 2.4. These responses are denoted by "FEM + MSKE". In addition, circles, which are denoted by "Direct FEM", are responses calculated directly by using Eq. (18). Both the responses are qualitatively consistent. Moreover, both the responses can be considered to be quantitatively consistent under $\eta_e \leqslant 0.5$ and $-\chi_e \leqslant 0.5$ in practice. This reveals the validity of the approximated modal damping in Section 2.4.

It took about 8 min to calculate the responses for one frequency by solving Eq. (18) in Fig. 15. Therefore, it required 8×9001 min to obtain the responses ranging from 100 to 1000 Hz with increment in frequency 0.1 Hz. On the other hand, it is necessary about 30 min to compute the responses by using MSKE method. Thus, the computations performed by using the proposed MSKE method were about 1500 times faster than those performed by solving Eq. (18) to obtain these responses.

4. Conclusion

We have described a method for vibration analysis of automotive double walls with a porous material. By applying an asymptotic method to a complex eigenvalue problem to obtain modal parameters, expressions for

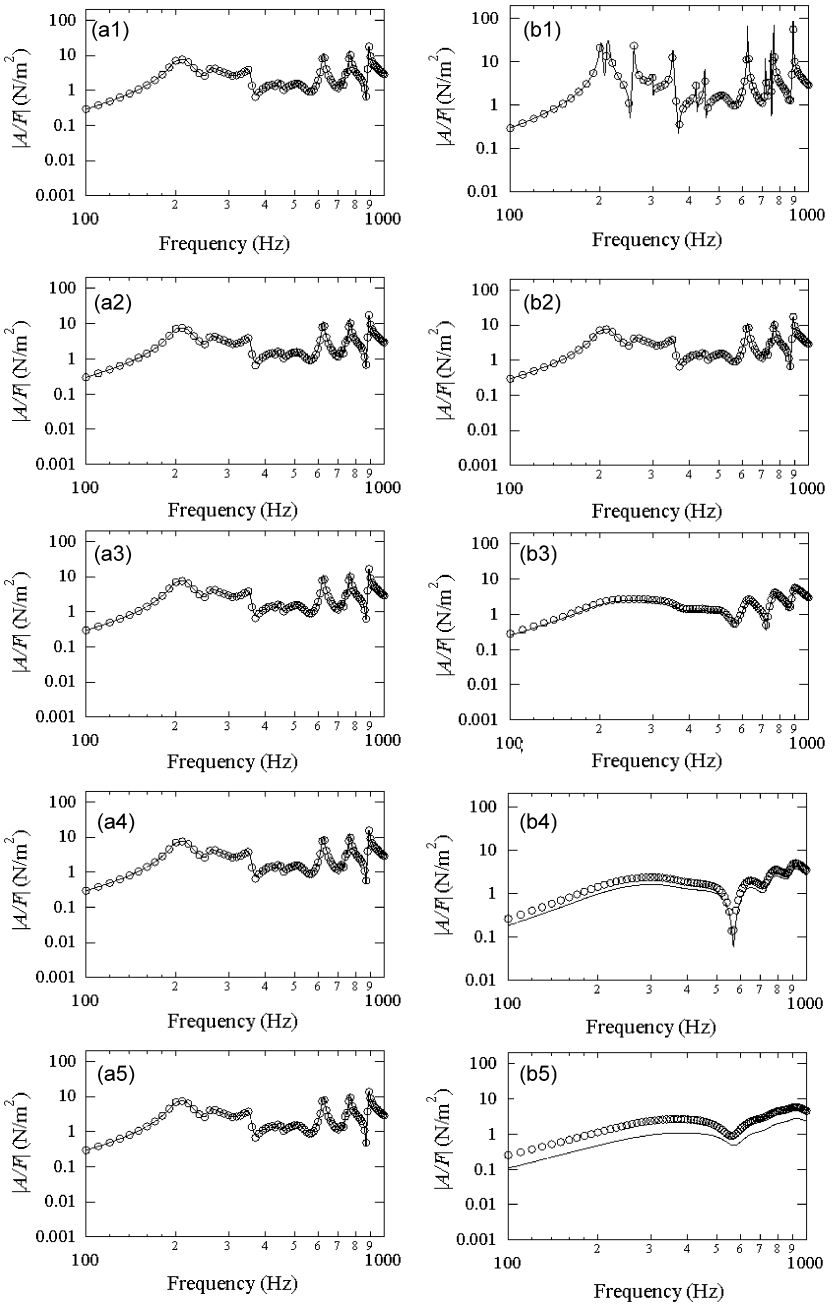

Fig. 15. Frequency responses calculated by modal strain and kinetic energy method: FEM + MSKE, —; direct FEM, ○: (a-1) $\eta_e = 0.1$, $\chi_e = -0.01$; (a-2) $\eta_e = 0.1$, $\chi_e = -0.1$; (a-3) $\eta_e = 0.1$, $\chi_e = -0.5$; (a-4) $\eta_e = 0.1$, $\chi_e = -1.0$; (a-5) $\eta_e = 0.1$, $\chi_e = -2.0$; (b-1) $\eta_e = 0.01$, $\chi_e = -0.1$; (b-2) $\eta_e = 0.1$, $\chi_e = -0.1$; (b-3) $\eta_e = 0.5$, $\chi_e = -0.1$; (b-4) $\eta_e = 1.0$, $\chi_e = -0.1$; and (b-5) $\eta_e = 2.0$, $\chi_e = -0.1$.

the modal loss factor are derived for three-dimensional damped structures. We developed the code by following the proposed approach. Further, we showed that computations performed by using the proposed MSKE method are 1500 times faster than those performed by solving discrete equations directly for responses ranging from 100 to 1000 Hz with increment in frequency of 0.1 Hz for a typical three-dimensional model of a damped structure.

The validity of responses to the MSKE method for three-dimensional damped structures was confirmed quantitatively under $\eta_e \leqslant 0.5$ and $-\chi_e \leqslant 0.5$ in practice.

There exist damping couplings between structures containing solid materials and porous materials for double walls filled with a porous material.

References

[1] P.M. Morse, K.M. Ingard, *Theoretical Acoustics*, Princeton University Press, Princeton, NJ, 1986.

[2] M. Gensane, F. Santon, Prediction of sound fields in rooms of arbitrary shape, *Journal of Sound and Vibration* 63 (1) (1979) 97–108.

[3] D.A. Bies, S. Hamid, In situ determination of loss and coupling loss factors by the power injection method, *Journal of Sound and Vibration* 70 (2) (1980) 187.

[4] C.D. Johnson, D.A. Kienholz, Finite element prediction of damping structures with constrained viscoelastic layers, *AIAA Journal* 20 (9) (1982) 1284–1290.

[5] B.A. MA, J.F. HE, A finite element analysis of viscoelastically damped sandwich plates, *Journal of Sound and Vibration* 152 (1) (1992) 107–123.

[6] T. Yamaguchi, Y. Kurosawa, N. Sato, S. Matsumura, Vibration characteristics of damped laminates having three-dimensional shapes in automotive body panels, *Proceeding of the 17th International Congress on Acoustics*, Roma, Italy, September 2001.

[7] Y. Kurosawa, S. Matsumura, H. Enomoto, T. Yamaguchi, High frequency vibration analysis of automotive bodies with panels that have attached viscoelastic layers, *Proceedings of 2003 ASME International Mechanical Congress & Exposition*, *IMECE2003-43839*, Washington, DC, USA, November 2003, pp. 25–30.

[8] S. Sato, T. Fujimori, H. Miura, Sound absorbing wedge design using flow resistance of glass wool, *Journal of the Acoustical Society of Japan* 33 (11) (1979) 628–636.

[9] K. Ejima, T. Ishii, S. Murai, The modal analysis on the acoustic field, *Journal of the Acoustical Society of Japan* 44 (6) (1988) 460–468.

[10] K. Yuge, R. Ejima, R. Udagawa, Y. Kishikawa, K. Kasai, Sound insulation analysis of a resin using viscoelastic constitutive equations, *Transactions of Japan Society of Mechanical Engineers* 60 (570A) (1994) 535–552.

[11] C. Zwikker, C.A. Kosten, *Sound Absorbing Materials*, Elsevier Press, Amsterdam, 1949.

[12] J.F. Allard, *Propagation of Sound in Porous Media*, Elsevier Applied Science, London and New York, 1993.

[13] H. Utsuno, T. Tanaka, T. Fujikawa, Transfer function method for measuring characteristic impedance and propagation constant of porous materials, *Journal of the Acoustical Society of America* 86 (2) (1989) 637–643.

[14] H. Utsuno, T.W. Wu, A.F. Seybert, T. Tanaka, Prediction of sound fields in cavities with sound absorbing materials, *AIAA Journal* 28 (11) (1990) 1870–1875.

[15] H. Utsuno, T. Tanaka, Y. Morisawa, T. Yoshimura, Prediction of normal sound absorption coefficient for multi layer sound absorbing materials by using the boundary element method, *Transactions of Japan Society of Mechanical Engineers* 56 (532C) (1990) 3248–3252.

[16] T. Yamaguchi, Approximated calculation to damping properties of a closed sound field involving porous materials, *Transactions of Japan Society of Mechanical Engineers* 66 (648C) (2000) 2563–2569.

[17] T. Yamaguchi, Y. Kurosawa, S. Matsumura, Damped analysis of 3D acoustic fields involving sound absorbing materials using FEM, *Transactions of Japan Society of Mechanical Engineers* 66 (646C) (2000) 1842–1848.

[18] M.A. Biot, Theory of propagation of elastic waves in a fluid-saturated porous solid, *Journal of the Acoustical Society of America* 28 (2) (1955) 168–178.

[19] Y.J. Kang, S. Bolton, Finite element modeling of isotropic elastic porous materials coupled with acoustical finite elements, *Journal of the Acoustical Society of America* 98 (1) (1955) 635–643.

[20] N. Attala, R. Panneton, P. Debergue, A mixed pressure-displacement formulation for poroelastic materials, *Journal of the Acoustical Society of America* 104 (3) (1998) 1444–1452.

[21] Y. Kagawa, T. Yamabuchi, A. Mori, Finite element simulation of an axisymmetric acoustic transmission system with a sound absorbing wall, *Journal of Sound and Vibration* 53 (3) (1977) 357–374.

[22] A. Craggs, A finite element model for rigid porous absorbing materials, *Journal of Sound and Vibration* 61 (1) (1978) 101–111.

[23] Y. Kiyota, M. Asai, H. Sugita, A. Akiyama, Low frequency noise reduction by improving sound insulation materials, SAE Paper, 951241, 1955, pp. 57–62.

[24] O.C. Zienkierwicz, Y.K. Cheung, *The Finite Element Method in Structural and Continuum Mechanics*, McGraw-Hill, New York, 1967.

[25] J.D. Ruzicka, *Structural Damping*, ASME, New York, 1959.

[26] E.L. Wilson, R.L. Taylor, W.P. Doherty, J. Ghaboussi, Incompatible displacement methods, *Numerical and Computer Methods in Structural Mechanics*, Academic Press, New York, 1973.

[27] T. Yamaguchi, Y. Kurosawa, S. Matsumura, FEM for damping of structures having elastic bodies, viscoelastic bodies, porous media and gas, *Mechanical Systems and Signal Processing* 21 (2007) 535–552.